2007-01-1370

Monitoring the Effect of RSW Pulsing on AHSS using FEA (SORPAS) Software

I. Khan, M. L. Kuntz and Y. Zhou
University of Waterloo

K. Chan and N. Scotchmer
Huys Industries Ltd.

ABSTRACT

In this study, a finite element software application (SORPAS®) is used to simulate the effect of pulsing on the expected weld thermal cycle during resistance spot welding (RSW). The predicted local cooling rates are used in combination with experimental observation to study the effect pulsing has on the microstructure and mechanical properties of Zn-coated DP600 AHSS (1.2mm thick) spot welds. Experimental observation of the weld microstructure was obtained by metallographic procedures and mechanical properties were determined by tensile shear testing. Microstructural changes in the weld metal and heat affect zone (HAZ) were characterized with respect to process parameters.

INTRODUCTION

In recent years, automotive manufacturers have successfully introduced high strength steels (HSS) into the automobile architecture, resulting in improved occupant safety through better crash performance. There is a current drive to increase the percentage of higher strength-to-weight-ratio materials to reduce autobody weight, and thus reduce energy consumption and emissions. The use of advanced high strength steels (AHSS) for structural components accomplishes this and further propagates light-weighting objectives through mass compounding (i.e. mass reduction in other vehicle systems with decreased body weight). One of the difficulties with substituting AHSS for low-alloy steels is that joining these materials presents challenges [1]. The microstructure of AHSS results in mechanical properties that are ideal for automotive applications with high strength and good ductility; however, microstructural changes during welding dramatically affect mechanical properties by transforming the base metal microstructure. Resistance spot welding is the primary sheet metal welding process in the manufacture of automotive assemblies. The mechanical and metallurgical changes in AHSS after the resistance spot welding operations are well-documented in the literature [2,3,4]; however, much work is left to be done to improve the quality and attain optimal mechanical properties. For example, excessive hardening or softening in the weldments of dual phase (DP) steels can result in decreased strength or toughness of the joint [5]. Improving weld performance is essential to the integration of AHSS sheet in future automobiles.

Mechanical properties of the weldment can be modified to better suit the application by tailoring the thermal cycle during RSW. This is typically accomplished by the addition of multiple pulses to the weld procedure. Pulsing enables control of heating and cooling rates during RSW; which in turn, affects the size and microstructure of the weld. In this study the effects of pulsing on the mechanical properties of resistance spot welded DP600 are examined. Numerical simulations are used to simulate the weld thermal cycle, and the results are analyzed to better understand the effects of pulsing on the microstructure.

EXPERIMENTAL PROCEDURES

The chemical properties of the material used in this study are summarized in Table 1. The RSW samples were produced using a Centerline Ltd. 250-kVA pneumatically operated single phase RSW machine with constant current control and a frequency of 60 Hz. A truncated class 2 electrode with 6.0 mm face diameter was used as per AWS standards for 1.22 mm thick sheet [6]. Cooling water flow rate followed AWS recommendation of 4 l/min. An extended hold time of 30 cycles was used to accommodate SORPAS limitations. The RSW machine was fully equipped with a DAQ system capable of recording load, displacement (±0.01 mm), current and voltage simultaneously as a function of time. A linear transducer mounted to the top electrode measures the displacement while a calibrated coil collects the dI/dt, which is conditioned to attain current as a function of time. The load cell located under the bottom electrode measures the force applied by the overhead cylinder. The data acquisition rate was 25,000 points per second (pps). Figure 1 a) shows the typical DAQ output for dual pulse resistance spot weld.

Table 1: DP600 Material Properties

[illegible]	[illegible]	[illegible]	[illegible]	[illegible]	[illegible]	[illegible]	[illegible]
DP600	1.22 mm	HDG	0.1	1.523	0.195	0.197	0.156

In an initial study single-pulse RSW samples were produced over a range of force, current, and time parameters. A weldability test was conducted to determine weld lobes which produce acceptable weld quality as determined by AWS standards [6]. The weld current was varied from 7 to 9kA, the weld force ranged from 3.5 to 5.5 kN, and the weld time was between 10 and 20 cycles. The weld parameters optimized for tensile shear strength and button size were 8kA, 3.5 kN, and 20 cycles. The weld samples were subjected to overlap tensile shear testing, coach peel testing, and metallographic examination. A total of 11 tests were conducted per condition including 5 tensile tests, 5 peel tests and 1 sample for metallographic preparation. Optimal mechanical properties were attained using the 8kA current, 3.5 kN force and 20 cycle weld.

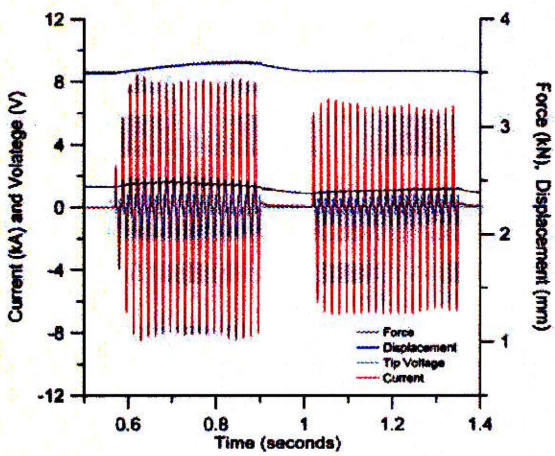

a) Typical DAQ output

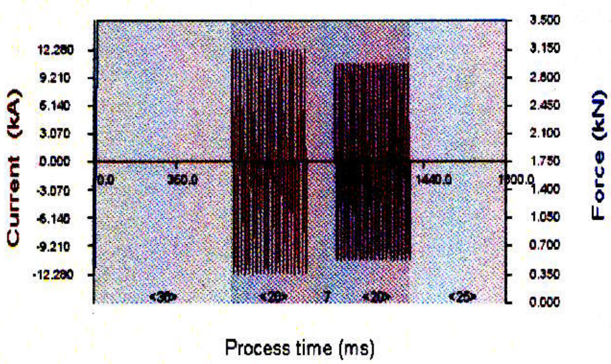

b) SORPAS simulation parameters

Figure 1: Experimental outputs and simulation parameters

For the two pulse weld schedule, the current, force and time for the initial pulse were maintained at 8kA, 3.5 kN and 20 cycles, respectively. The second pulse followed after a 7 cycle hold period, the 3.5 kN force and 20 cycle weld time were maintained, while the current varied from 1kA – 8kA. Table 1 summarizes the welding schedule used. A total of six samples were prepared for each condition, including five tensile shear test specimens and one for micro-hardness testing.

An Instron tensile testing machine was used for shear testing at a constant crosshead velocity of 10mm/min. Displacement values were attained at the failure load. Energy absorbed during tensile testing was calculated by integrating the load displacement curve to failure. Equation 1 was used to find the energy during tensile loading.

$$Q = \sum_{n=1}^{N} F(n) \cdot \left(x(n) - x(n-1) \right) \qquad (1)$$

Where the product of force (F) and displacement (x) are summed for each data set sampled (N) up to the failure load.

During metallographic examination all test sections were etched using Lepera's reagent to distinguish the different phases in the base metal, heat affected zone and fusion zone [7]. When this particular etchant is used, martensite is etched white, alpha-ferrite is tan-colored and bainite is black.

Microhardness testing of DP600 steel sheet was carried out using a Clemex MT-2001 Vickers micro-hardness testing machine using a 200 g load and a holding time of 15 seconds. Microhardness mapping using 0.2 mm grid spacing revealed the hardness distribution and the individual hardness values in selected regions of welded joints.

SIMULATION PARAMETERS

Numerical simulations were carried out using *SORPAS®* Enterprise Edition 7.0 FEA software from *Swantec Software and Engineering ApS* [8]. The typical simulation mesh is shown in Figure 2. Welding electrodes and work sheet configurations were entered into the simulation using a 2D co-ordinate mapping system to create objects. A materials database is then used to assign the object material properties. Once the objects have been created, the machine tools were specified to apply the specified weld force, current and time. A mesh of 1500 nodes was applied to the 2D image with a denser mesh near the interface of the material.

The weld force, current and time was characterized to match the experimental set up as shown in Figure 1. It is important to note that the current version of SORPAS requires the electrodes to remain in contact with the worksheet after a weld is completed. Hence, to maintain consistency and attain accurate results a post-weld hold time of 30 cycles was necessary during laboratory testing.

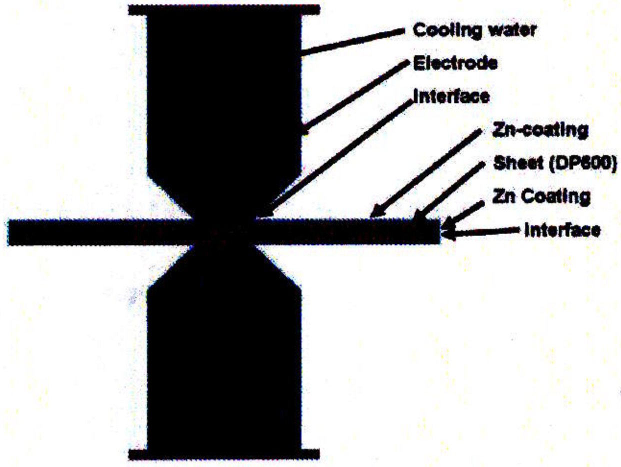

Figure 2: Simulation mesh and mesh geometry

The actual geometry of the electrode was measured and replicated in SORPAS. Cooling water was set at 9°C to simulate the laboratory cooling water temperature. Furthermore the measured thickness of Zn-coating was input on the sheet surfaces. Constant current settings were selected to match the experimental methods. Simulation input parameters for SORPAS are shown in Table 2.

Table 2: Welding schedule

[redacted]	Squeeze	1st Pulse	Hold	2nd Pulse	Hold
[redacted]	-	8kA	-	1kA – 8kA	-
[redacted]	25	20	7	20	30

EXPERIMENTAL RESULTS AND DISCUSSION

In order to understand the effect of weld schedule on material properties the weld metallurgy of DP600 must first be considered. A representative single-pulsed RSW cross-section is shown in Figure 3 (8kA, 3.5kN, 20cycles). The fusion zone (FZ), heat affected zone (HAZ) and base metal (BM) can be clearly observed. Microstructural observations of these regions are shown in Figure 3a) to d). The BM in Figure 3a) shows the typical finely dispersed martensite particles (white) surrounded by a ferrite matrix (light gray) that are characteristic of the automotive dual-phase steels. Peak temperatures during welding in this region are typically below the martensite tempering temperature (i.e. less than 200°C). In the HAZ, the volume fraction of martensite increased. The peak temperature during welding in this region ranges from martensite tempering temperatures to just below the liquidus. Figure 3b) shows a transitional area from the intercritical (IC) to the fine grained region (FG) within the HAZ. Peak temperatures in the IC region are between the Ac1 and Ac3, resulting in a coarsening of the martensite phase. Within the FG region, temperatures exceed the Ac3 resulting in complete austenitization. The austenite is inhomogeneous due to the nature of segregation within the DP microstructure and short time above Ac3; resulting in the banding nature of martensite and the formation of fine grained ferrite. Closer to the fusion boundary, the peak temperature is well above Ac3, resulting in complete austenitization and grain growth. The coarse grain (CG) region consists of prior austenite grains about 10-15 μm in diameter. The microstructure in the CG region is blocky martensite, as shown in Figure 3c). The FZ shown in Figure 3d) is characterized by the columnar nature of solidification. The microstructure in the FZ consists of large equiaxed columnar martensite grains.

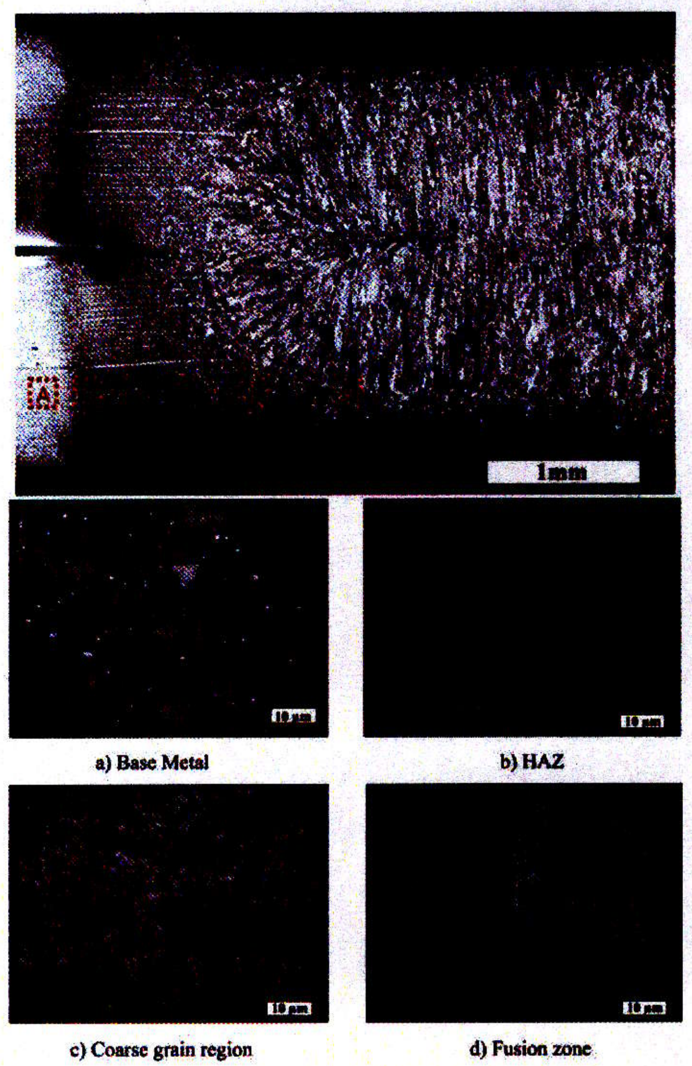

Figure 3: Microstructure of various weld regions [10]

Simulation results for temperature during welding are compared side-by-side with a weld cross section of a single pulse weld in Figure 4. The fusion zone is outlined in violet, the CG HAZ is outlined in red, and the IC HAZ is outlined in green. The size and shape of the weld sub-regions shows good agreement with the simulation output. Individual mesh nodes at the weld centerline

(CL), edge of the FZ, and in the CG and IC HAZ are identified in Figure 4. The location of these nodes is used to compare the thermal history within the sub-regions for different weld parameters. The single pulse temperature-time profile for individual nodes in the FZ, CG HAZ and IC HAZ are shown in Figure 5. The predicted FZ peak temperature of 1605 °C is above the liquids temperature for this steel alloy. For the CG region the temperature range is typically 1100-1300°C and the predicted peak temperature at the reference node is 1362 °C. The IC region peak temperature was predicted to be 880 °C and typically range from Ac1 and Ac3 (~730 °C -900 °C).

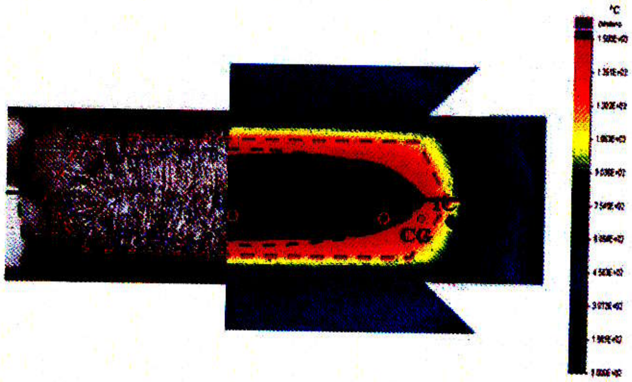

Figure 4: Simulation output at peak temperature

The microstructure of the weld sub-regions is largely dependent upon the local thermal history during welding, and to a significant extent, the cooling rate during the transformation temperature range. As the cooling rate varies with temperature, it is often more convenient to express the thermal history as the time required to cool between two temperatures. For instance, the time required for cooling from 800 °C-500 °C ($\Delta t_{8/5}$) is widely used to help predict the microstructure and mechanical properties during welding of conventional steels [9]. This time can then be compared to the time required to reach the ferrite-pearlite nose on a continuous cooling-transformation (CCT) diagram. Thus, the likelihood of forming either a ferritic or martensitic structure can be predicted. Figure 5 shows how this transformation time is determined in the CG HAZ weld region using the simulated thermal history. In this study $\Delta t_{8/5}$ is used as a starting point for comparing thermal histories between welds produced with different schedules. It is important, however, to note that the high alloying content coupled with unique material processing techniques is expected to alter the transition temperatures for DP600 AHSS.

Figure 6 shows the modeled temperature profiles at the reference nodes for the full range of second pulse currents. Addition of a second pulse alters the thermal history for the various regions in the weld. With increasing pulse current, the cooling rate during the pulse time decreases up to 4kA. Above a second pulse current of 4kA reheating is predicted to occur in all weld regions. Figure 6 a) and b) show temperatures reaching above the liquidus at a second pulse current of 7kA and 8kA causing re-melting to occur in the FZ. In the CG region, Figure 6 c), the liquidus temperature is exceeded with an 8kA second pulse. In this case, the FZ re-melts and the weld nugget grows into the HAZ. The time-temperature profile for the IC sub-region shows temperatures above the Ac3 for extended periods of time for higher currents indicating growth of the HAZ. The final microstructure at this node is expected to be CG HAZ when the second pulse current is greater than 7kA. Clearly, the addition of a second pulse changes the local thermal history in the weld regions with an expected impact on weld properties.

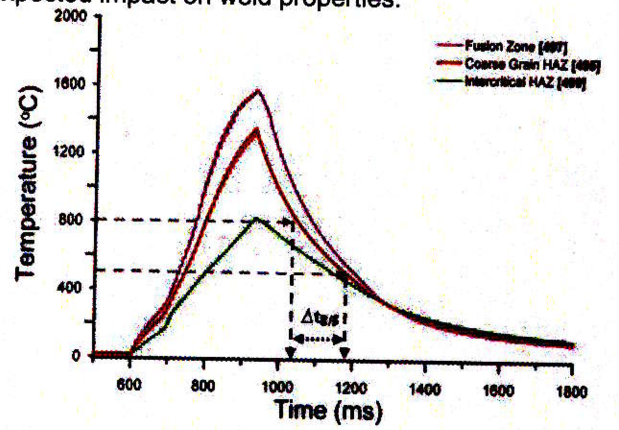

Figure 5: Temperature-Time profile for various weld zones

The predicted $\Delta t_{8/5}$ as a function of second pulse current for the CL, FZ and CG nodes is shown in Figure 7. With increasing current, $\Delta t_{8/5}$ increases up to 4kA for all regions. In the FZ, $\Delta t_{8/5}$ decreases sharply beyond 4kA, then gradually increases again with current. In the CG region, $\Delta t_{8/5}$ decrease sharply when the second pulse current exceeds 5kA pulse and also increases gradually with current. From Figure 7 it can also be shown that the transformation time decreases from the HAZ to CL.

The simulated cooling rates from Figure 7 can be used to predict the effects of pulsing on weld microstructure and hardness. It is well known that increased transformation time aids in decreasing the hardness of the martensitic microstructure. As the pulse current is increased up to 4kA, softening is expected to occur in both the FZ and HAZ. The sharp decrease in $\Delta t_{8/5}$ at 5kA is expected to produce a significantly harder FZ microstructure. Beyond 5kA the FZ microstructure is expected to soften with increased current. A similar trend is expected in the HAZ.

Results of hardness mapping from the weld centerline to base material are shown in Figure 8. The profiles include the BM, HAZ, and FZ regions for the 1kA through 8kA second pulse currents. Hardness values are lowest in the BM (left) and increase approaching the FZ (right). BM hardness ranges between 150-200HV while the IC HAZ consists of a 200-250HV region. The CG and FZ hardness values range above 250HV.

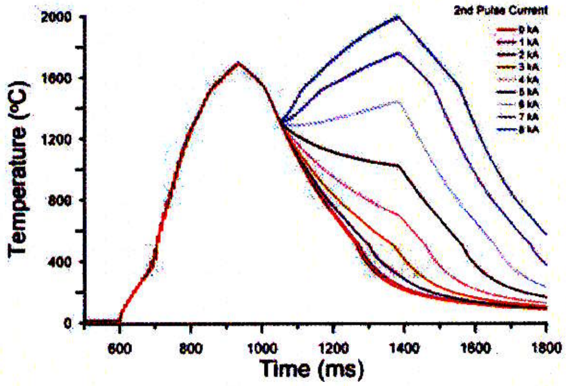

a) Weld Centerline [CL]

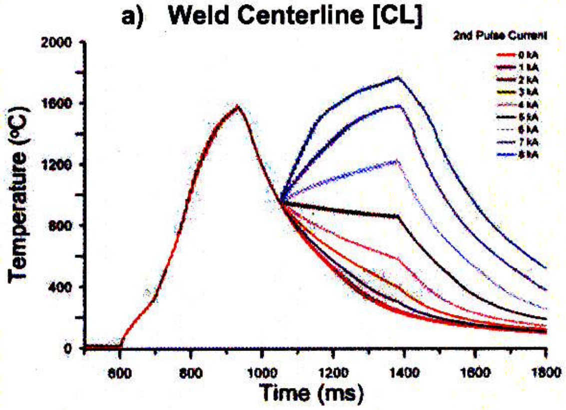

b) Fusion zone [FZ]

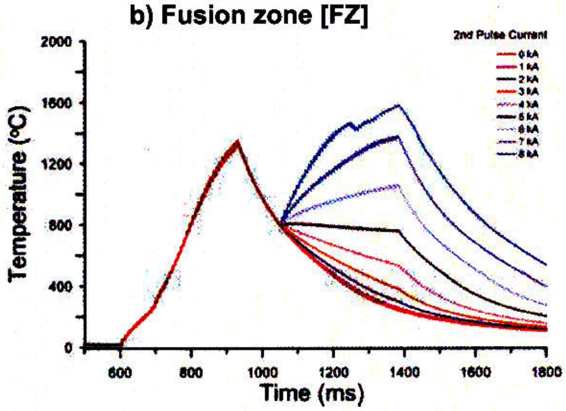

c) Coarse grain HAZ [CG]

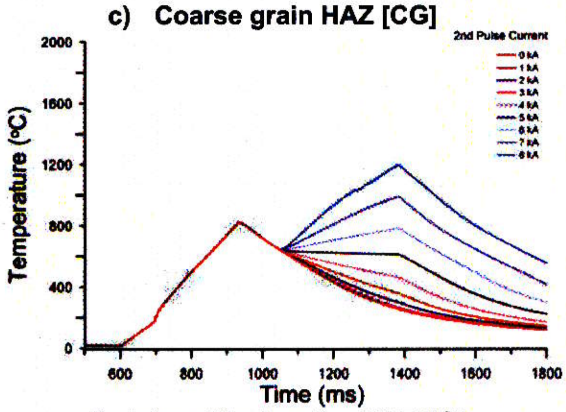

d) Intercritical region HAZ [IC]

Figure 6: Temperature time graph for referenced weld zones

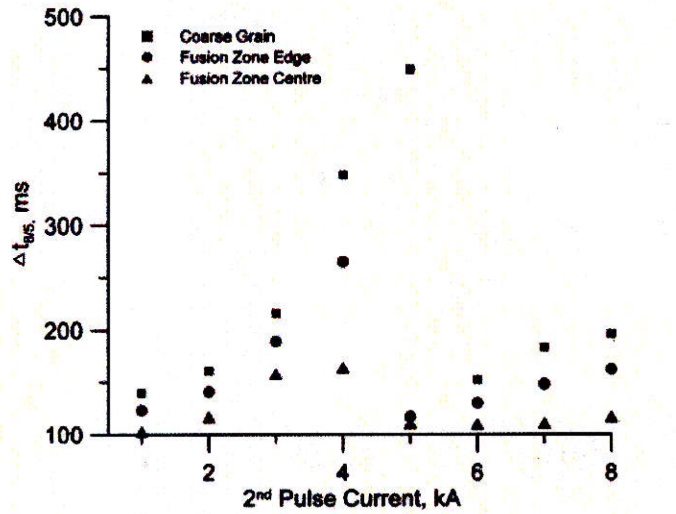

Figure 7: $\Delta t_{8/5}$ for various weld zones

Figure 8 shows how variation of the second pulse current affects the measured hardness values. Increasing the second pulse current from 1kA to 2kA results in softening of the FZ microstructure. This suggests an increase in the transformation time and autotempering of the martensitic structure during cooling. The results of the weld simulation support this result. As the second pulse current is increased to 4kA, there is a notable increase in the measured FZ hardness. These results suggest a higher cooling rate through the transformation temperature range and reduced autotempering of the fusion zone microstructure. When the pulse current is increased beyond 4kA to 5kA, the measured microstructure decreases significantly. There is some disagreement with the expected results as Figure 7 shows an increase in cooling rate between 800 °C and 500 °C, and thus an expected harder FZ microstructure at 5kA, rather than the observed 4kA second pulse current. Further increase of the second pulse current through to 8kA results in additional softening of the FZ microstructure, as predicted by the simulation results which show decreased cooling rates and increased autotempering of the microstructure. Increasing FZ size is shown in Figure 8 g) to h) and is also predicted in Figure 6, which shows peak temperatures exceeding the liquidus for the CG HAZ during the 8kA pulse. Although there is some disagreement with the hardness trends predicted from the simulation results, the general pattern is consistent with expectations. Further investigation could yield a more suitable transformation temperature range that reflects observed microstructural tendencies in pulsed RSW schedules.

Mechanical testing results from overlap shear testing are shown in Figure 9. Full interfacial fracture (FIF) was observed with all samples. There is no significant observed effect of second pulse current on failure load; however, at 4kA a decrease in strength to failure is observed. The high measured hardness values at this current suggest the decrease could be related to fracture mechanics. Beyond the 5kA pulse an increase in failure load despite a softer FZ microstructure is likely a result of the increase in fusion zone weld area. Previous studies on DP600 have shown an increase in failure loads as the bonded area of the FZ increases [10]. Optimal weld quality was achieved using the 2kA second pulse, which exhibited the highest strength and ductility. There is a decrease in energy absorption and displacement beyond the 2kA pulse.

Since all fractured samples exhibited FIF, the main focus lies in microstructure and mechanical properties in the FZ. Optimal mechanical properties were achieved with the 2kA second pulse, which produced a balance between hardness and ductility. Lower cooling rates result in auto-tempering of the martensite at lower temperatures. At a 4kA second pulse current, high cooling rates produce the hardest microstructure with poor ductility. For a second pulse current of 8kA, softening of the FZ is a result of low cooling rates. The reduced ductility observed at higher second pulse currents may be related to the re-solidification microstructure and larger grain size.

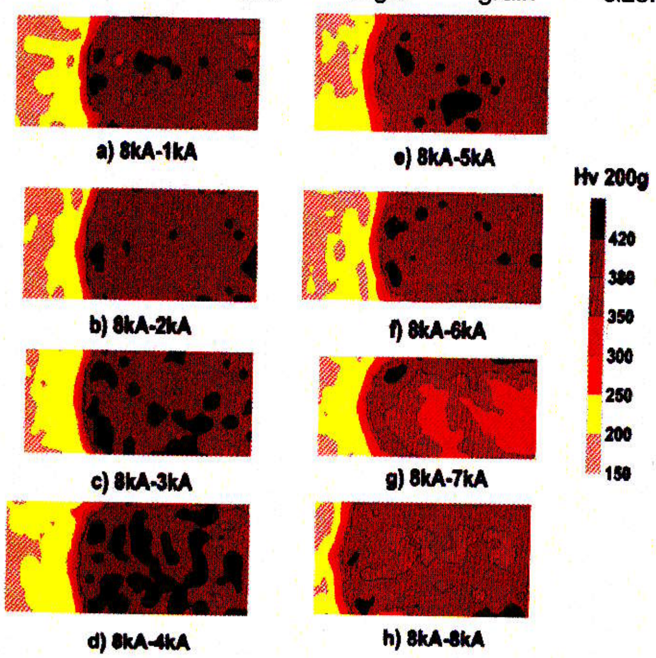

Figure 8: Hardness mapping of RSW weld

Using the results of RSW simulations, the effects of varying the second pulse current on thermal history and corresponding microstructure/mechanical properties can be observed. It has been pointed out that the cooling time between 800°C - 500°C may not be the best choice for this alloy and welding process. The higher levels of alloying elements found in AHSS may require a lower temperature range for transformation. Hence, this would lead to the longer transition time for lower currents and perhaps an improved prediction. Additional work is required to determine if a suitable temperature range for cooling time can be found for predicting microstructure. Furthermore, the relationship between mechanical properties and microstructure requires further exploration in order to enable optimization through simulation.

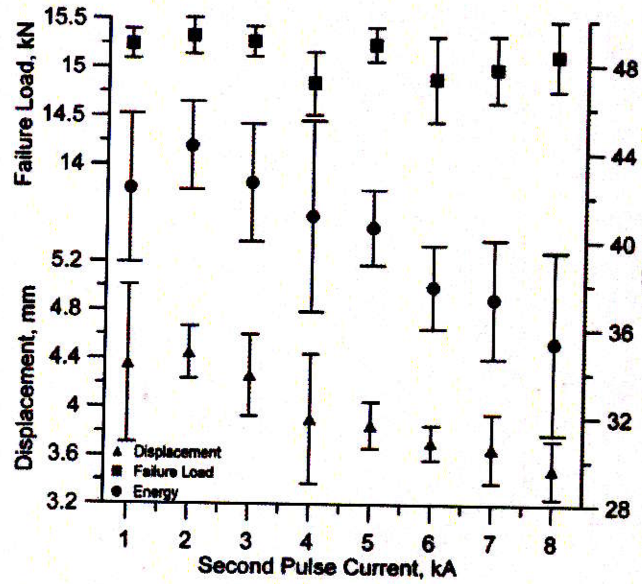

Figure 9: Failure load, displacement and energy absorbed for varying second pulse current

CONCLUSION

The effects of varying the current of the second weld pulse of a RSW schedule on the microstructure and mechanical properties of DP600 AHSS sheet have been evaluated using numerical simulations and laboratory experiments. The weld properties of resistance spot welded DP600 AHSS were investigated using a combination of metallographic examination, micro-hardness testing, and overlap tensile shear testing. The effect of the second pulse current on the thermal history of different regions in the weld has been evaluated using SORPAS finite element analysis and data acquisition of key welding parameters. The results have shown that:

1) Varying the second pulse current in a pulsed RSW schedule can be used to modify the weld thermal cycle and alter the cooling rate during RSW.

2) The size and hardness of the fusion zone and heat affected zone is influenced by the local thermal history, and can be controlled by the pulse current.

3) Weld performance in tensile shear testing including: load to failure, displacement and energy absorption can be optimized by selecting an appropriate pulse schedule.

4) Weld simulation tools can be used to analyze weld thermal cycles and optimize weld schedules for mechanical properties; however, additional work is required to determine temperature-time transformation characteristics of AHSS, and develop relationships between microstructure and mechanical properties.

ACKNOWLEDGMENTS

The authors wish to acknowledge financial support from Auto21 and Dofasco for providing material for testing and use of equipment.

REFERENCES

1. A/SP AHSS Applications Recommendations, February 8, 2005

2. Kunishige, K., Yamauchi, N., Taka T. and Nagao, N. 1983. Softening in Weld Heat Affected Zone of Dual Phase Steel Sheet for Automotive Wheel Rim, SAE Technical Paper Series #830632, *SAE Int. Congress & Exposition, Detroit, MI, Feb 28-Mar 4.*

3. Ghosh, P.K., Gupta, P.C., Pal, O.M., Avtar, R., Jha, B.K., and Sagar Dwivedi, V. 1993.Influence of Weld Thermal Cycle on Properties of Flash Butt Welded Mn-Cr-Mo Dual Phase Steel. *ISIJ Int.* 33 (7): 807-815.

4. Ghosh, P.K., Gupta, P.C., Avtar, R., and Jha, B.K. 1991. Weldability of Intercritical Annealed Dual-Phase Steel with the Resistance Spot Welding Process. *Weld. J.* 70 (1):7-s to 14-s.

5. Tawade, G. and Boudreau, G., "Robust Schedules for Spot Welding Zinc-Coated High Strength Automotive Steels," *Great Design in Steel* (2004).

6. ANSI/AWS/SAE/D8.9-97, "Recommended Practices for test methods for evaluating the resistance spot welding behavior of automotive steels", AWS/SAE, 1997

7. Frank S. Lepera, Improved etching technique to emphasize martensite and bainite in high-strength dual-phase steel, pp 38-39, Journal of Metals, March, 1980.

8. Swantec Software and Engineering ApS, Denmark, www.swantec.com

9. Kou, S. (2002). Welding Metallurgy, Wiley: pg:234-235.

10. I. Khan, M. L. Kuntz, P. Su, A. Gerlich, T. North and Y. Zhou," Resistance and Frisction Stir Spot Welding: A comparative study", Science and Technology of Welding and Joining, accepted September 2006.

CONTACT

Professor Norman Zhou, Department of Mechanical Engineering, University of Waterloo.
nzhou@mecheng1.uwaterloo.ca
(519)888-4567, ext. 6095.